CFD PROJECT REPORT

2D UNSTEADY INCOMPRESSIBLE FLOW PAST CIRCULAR CYLINDER

DE-43-ME-A

Saad Ahmad

Ahmed Saeed

Ali Akhtar

TO:

DR. TARIQ TALHA

NUST, Islamabad

Table of Contents

Numerical Analysis and Validation of Two-Dimensional Unsteady Incompressible Flow Around a Stationary Circular Cylinder at Re = 100

Saad Ahmad[a] , Ahmed Saeed[b], Ali Akhtar[c]

[a]*Department of Mechanical Engineering, NUST, Pakistan,* saadah.me43ceme@student.nust.edu.pk

[b]*Department of Mechanical Engineering, NUST, Pakistan* ahmed.saeed.study@gmail.com

[c]*Department of Mechanical Engineering, NUST, Pakistan* aakhtar.me43ceme@nust.edu.pk

ARTICLE INFO

Keywords:

Circular cylinder

Incompressible flow

Numerical simulations

Low Renold's number

ABSTRACT

This investigation aims to carry out a numerical study of a two-dimensional[1] unsteady incompressible flow over a stationary circular cylinder at a Reynolds number of 100[2] using ANSYS software. Some of the analysis includes simulation of velocity fields, continuity and momentum equations convergence assessment, and pressure distributions assessment. To do this, the pressure coefficient (c_p) is calculated and then matched with literature values to check the results. Processes aimed at achieving grid independence are employed. Several of these processes relate to grid resolution and its effects on the outcome of numerical computations. Specific flow features such as vorticity contours, lift coefficient (c_l), and drag coefficient (c_d) are accurately and explicitly illustrated. Strouhal number (S_t), (c_l) root mean square, and mean drag coefficient (c_d) were calculated and matched with reference literature values. It is tied very strongly on theoretical concepts and experimental work indicating that the modeling employed is valid. This work adds in-depth knowledge of the flow behavior around circular cylinders and provides a validated procedure for uninherited CFD studies[3].

Introduction

The flow around a circular cylinder is a well-known issue in fluid mechanics, marked by intricate unsteady flow behaviors like vortex shedding, oscillations in drag and lift, and changes in pressure distribution. This topic holds considerable importance in engineering, particularly in the design of bridges, offshore structures, pipelines, and wind turbine towers. To enhance the performance and structural integrity of these systems, it is crucial to accurately predict and analyze flow parameters such as drag coefficient, lift coefficient, Strouhal number, and pressure coefficient. The main goal of this study is to conduct a thorough numerical analysis of the unsteady, incompressible flow around a circular cylinder at a Reynolds number of 100 using ANSYS, with an emphasis on validating numerical findings against established theoretical and experimental data. The study aims to simulate the velocity field, vorticity contours, and pressure distributions, carry out grid independence studies, and compute and validate flow characteristics like drag, lift, and Strouhal number. This research adds to the field of computational fluid dynamics (CFD) by offering a validated framework for exploring similar flows and enhancing the understanding of vortex dynamics and pressure interactions in unsteady cylinder flows.

The Navier-Stokes equations describe the motion of a fluid by applying the fundamental principles of mechanics (conservation of mass and momentum) to

a fluid element. We consider a small cubical fluid element in 3D Cartesian coordinates with dimensions dx, dy, dz and analyzes the forces acting on it. Newton's Second Law ($F = ma$) for the fluid element:

$$Net\ force\ on\ the\ fluid\ element = Rate\ of\ change\ of\ momentum\ of\ the\ fluid\ element.$$

For a fluid element, the forces include body force e.g., gravitational force, expressed as $\boldsymbol{\rho g}$, where ρ is the fluid density and g is the gravitational acceleration. And surface force due to pressure and viscous stresses.

The pressure at the point (x, y, z) in the fluid is p.

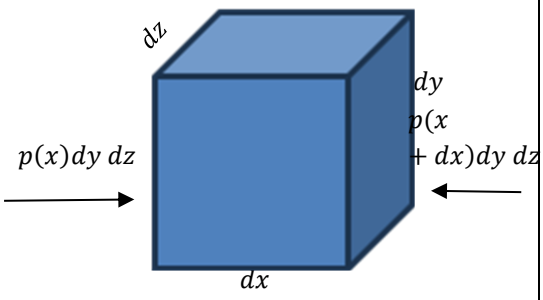

The pressure forces on the fluid are:

In $x - direction$, $p(x)A - p(x + dx)A$ where $A = dy\ dz$

Using Taylor series expansion, $p(x + dx) \approx p(x) + \frac{\partial p}{\partial x} dx$:

$$Net\ pressure\ force\ in\ x = -\frac{\partial p}{\partial x} dx\ dy\ dz$$

Similarly, forces in $y\ and\ z\ directions$ are:

$$-\frac{\partial p}{\partial y} dx\ dy\ dz, -\frac{\partial p}{\partial x} dx\ dy\ dz$$

Viscous forces are derived from the stress tensor τ_{ij}, representing shear & normal stresses in the fluid due to viscosity. The stress components are related to velocity gradients. Normal stresses are:

$$\tau_{xx} = 2\mu \frac{\partial u}{\partial x}, \tau_{yy} = 2\mu \frac{\partial v}{\partial y}, \tau_{zz} = 2\mu \frac{\partial w}{\partial z}$$

Shear stresses are:

$$\tau_{xy} = \tau_{yx} = \mu \left(\frac{\partial u}{\partial y} + \frac{\partial v}{\partial x} \right)$$

And similarly to other components. The net viscous force in each direction is calculated by considering the gradients of the stresses.

Summing up all forces in $x - direction$:

$$net\ force\ in\ x = -\frac{\partial p}{\partial x} + \mu \left(\frac{\partial^2 u}{\partial x^2} + \frac{\partial^2 u}{\partial y^2} + \frac{\partial^2 u}{\partial z^2} \right) + \rho g_x$$

Same for other directions. The rate of change of momentum per unit volume is:

$$\frac{Dv}{Dt} = \frac{\partial v}{\partial t} + v.\nabla v, \quad v = (u, v, w)$$

For incompressible flow $\nabla v = 0$, equating the forces to the rate of change of momentum, the Navier-Strokes equation is:

$$\frac{\partial v}{\partial t} + v.\nabla v = -\frac{1}{\rho} \nabla \rho + \nu \nabla^2 v + g$$

So, the tensor form of Navier-Strokes[4] will be, for each $i = 1,2,3$ *it is* $j = 1,2,3$

$$\frac{\partial u_i}{\partial t} + u_j \frac{\partial u_i}{\partial x_j} = -\frac{1}{\rho}\frac{\partial P}{\partial x_i} + \rho g_i + \frac{\mu}{\rho}\frac{\partial^2 u_i}{\partial x_j \partial x_j}$$

Literature Review

The study of flow past a circular cylinder, particularly at low to moderate Reynolds numbers, has been extensively explored in literature, providing valuable insights into the underlying flow dynamics. Investigations into steady and unsteady flow regimes have revealed the transition from steady-state flow to periodic vortex shedding at higher Reynolds numbers. For example, studies examining unsteady flows for Reynolds numbers up to 200 have shown the development of periodic vortex shedding patterns and discrepancies between various numerical methods, highlighting the need for further validation of lift, drag, and moment coefficients.

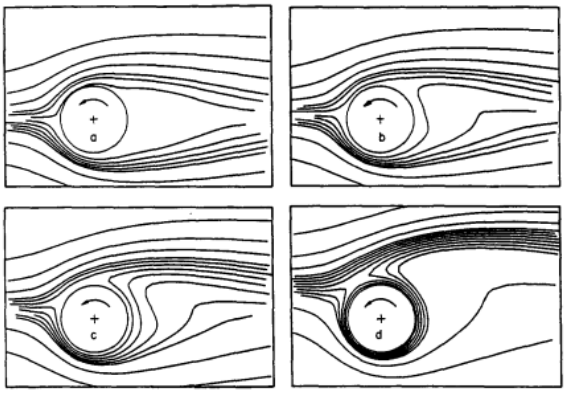

Figure 1 Pressure contours[5]

Research on wake instability has utilized advanced techniques like linear stability analysis and direct time integration to estimate critical Reynolds numbers and their sensitivity to computational parameters. The effect of domain boundaries and blockage ratio on the critical Reynolds number and Strouhal number further emphasizes the importance of accurate domain configuration and numerical resolution in such studies. This sensitivity underlines potential causes for discrepancies in past data, demonstrating the necessity of detailed parameter studies for reliable simulations.[6]

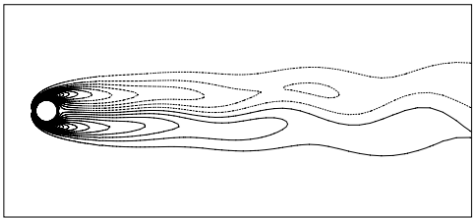

Fig. 4. Flow past a cylinder at $Re = 47.4$ with mesh H100R3: the top image shows the vorticity field reconstructed from the combination of the steady-state solution and the real and imaginary parts of the most unstable eigenmode. The lower image is the vorticity field from the 2D DTI. The broken lines denote negative while the solid lines represent positive value of the vorticity.

Additionally, finite-volume simulations at $Re = 100$ and beyond provide comprehensive datasets on force coefficients, velocity profiles, and vortex shedding characteristics. Observations such as non-monotonous streamwise velocity recovery and the influence of vortex dynamics in the wake reveal phenomena that have been overlooked in past studies. The transition to chaotic flow states at $Re = 200$, validated by three-dimensional simulations, emphasizes the complexity of flow behavior and the importance of multi-dimensional modeling for higher Reynolds numbers.

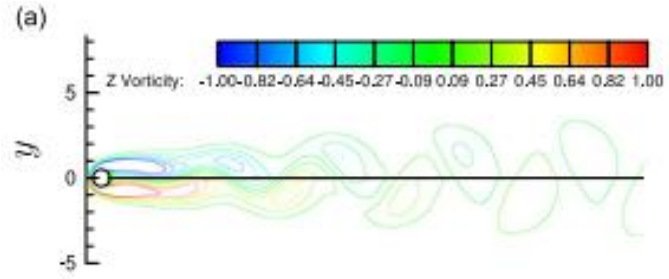

Figure 2 Instantaneous vorticity at Re=50[7]

While extensive studies have validated flow parameters for circular cylinders at higher Reynolds numbers, this study focuses on Reynolds number 100, providing a detailed comparison of pressure coefficients, lift, drag, and Strouhal number with literature. Additionally, a comprehensive grid independence analysis is performed to enhance the accuracy of simulation results.

Numerical Methodology

The governing equations for 2D unsteady incompressible flow past a circular cylinder[8], are:

The continuity equ. for incompressible flow is [9]

$$\nabla v = 0$$

Or

$$\frac{\partial u}{\partial x} + \frac{\partial v}{\partial y} = 0$$

This ensures the conservation of mass, meaning there is no net accumulation of fluid within a control volume.

For 2D incompressible flow, the Navier-Stokes equations in Cartesian coordinates are:

$x - direction$:

$$\frac{\partial u}{\partial t} + u\frac{\partial u}{\partial x} + v\frac{\partial u}{\partial y} = -\frac{1}{\rho}\frac{\partial p}{\partial x} + \frac{\mu}{\rho}\left(\frac{\partial^2 u}{\partial x^2} + \frac{\partial^2 u}{\partial y^2}\right)$$

$y - direction$:

$$\frac{\partial v}{\partial t} + u\frac{\partial v}{\partial x} + v\frac{\partial v}{\partial y} = -\frac{1}{\rho}\frac{\partial p}{\partial y} + \frac{\mu}{\rho}\left(\frac{\partial^2 v}{\partial x^2} + \frac{\partial^2 v}{\partial y^2}\right)$$

Simulation setup

The geometry of a 2D circular cylinder for analysis was made in design modular.

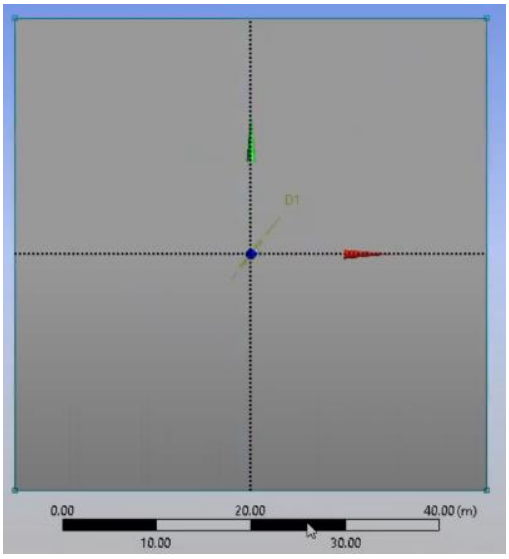

The proper edge sizing was done on face and edges of geometry. The first analysis was done for approximately 50,000 elements for enabling **transient (time-dependent) simulation** to capture unsteady flow features like vortex shedding and selecting the laminar model.

Details of "Edge Sizing" - Sizing

Scoping Method	Geometry Selection
Geometry	1 Edge
Definition	
Suppressed	No
Type	Element Size
Element Size	2.5e-002 m
Advanced	
Growth Rate	Default (1.2)
Capture Curvature	Yes
Curvature Normal Angle	Default (18.0°)
Local Min Size	Default (1.1979e-002 m)
Capture Proximity	No
Bias Type	No Bias

Details of "Face Sizing" - Sizing

Scoping Method	Geometry Selection
Geometry	1 Face
Definition	
Suppressed	No
Type	Element Size
Element Size	0.1 m
Advanced	
Defeature Size	Default (5.9896e-003 m)
Growth Rate	Default (1.2)
Capture Curvature	Yes
Curvature Normal Angle	Default (18.0°)
Local Min Size	Default (1.1979e-002 m)
Capture Proximity	No

The **inflation setting** is done to refine the mesh near walls or surfaces where boundary layers form. This is crucial for accurately capturing gradients in velocity, pressure, and other flow variables in regions of steep variation, such as near the surface of the cylinder in analysis.

Details of "Inflation" - Inflation

Scope	
Scoping Method	Geometry Selection
Geometry	1 Face
Definition	
Suppressed	No
Boundary Scoping Method	Geometry Selection
Boundary	1 Edge
Inflation Option	First Layer Thickness
First Layer Height	2.5e-002 m
Maximum Layers	20
Growth Rate	1.5
Inflation Algorithm	Pre

Boundary Conditions

The inlet conditions were applied to the initial velocity of the incompressible fluid, so that it must lie in the laminar region.

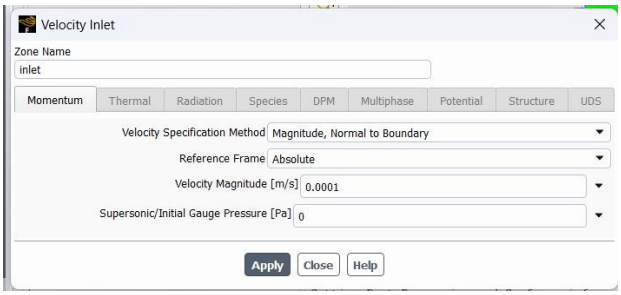

The outlet condition settings are these.

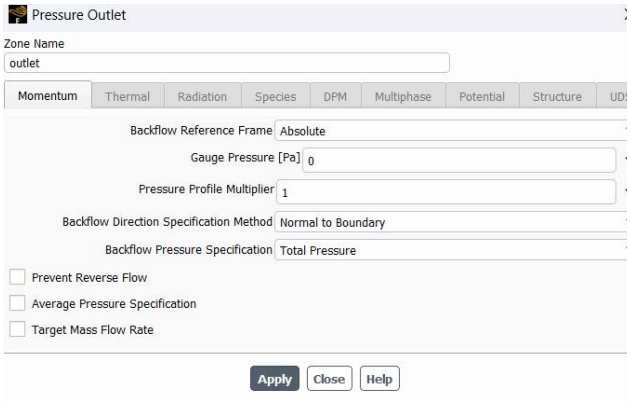

These conditions were applied to the boundary region of the 2D cylinder. The wall is considered stationary with no-slip conditions.

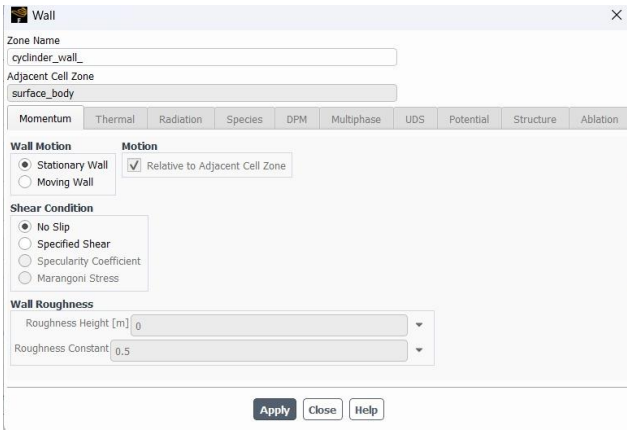

Mesh Generation

The mesh was generated of the 50,000 element sizing initially and later larger for mesh independent studies.

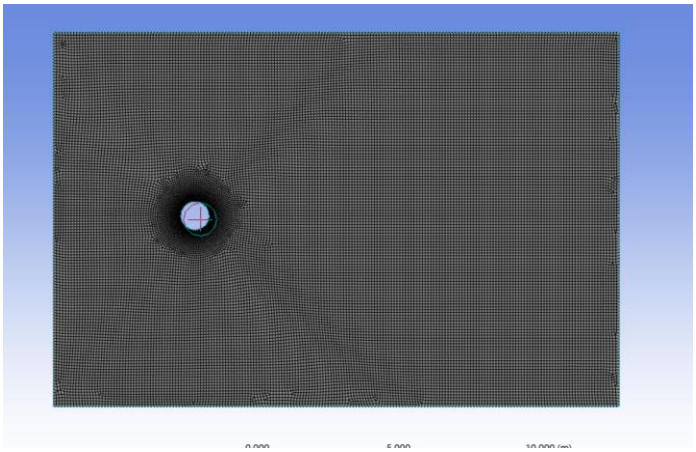

Figure 3 Mesh with 50,000 elements

Results

After the validation and verification from available literature the following are the results for numerical simulations with available experimental results for comparison.

Velocity Field Distribution

The velocity field reveals characteristic flow features for a circular cylinder at $Re = 100$. High-velocity regions are observed near the upper and lower surfaces of the cylinder, with stagnation occurring at the front. Flow separation occurs symmetrically on both sides, leading to the formation of a wake region with reduced velocity downstream. The periodic nature of vortex shedding is evident, consistent with the Strouhal number computed from the lift coefficient oscillations. The boundary layer development and separation points align closely with published results, validating the numerical model.

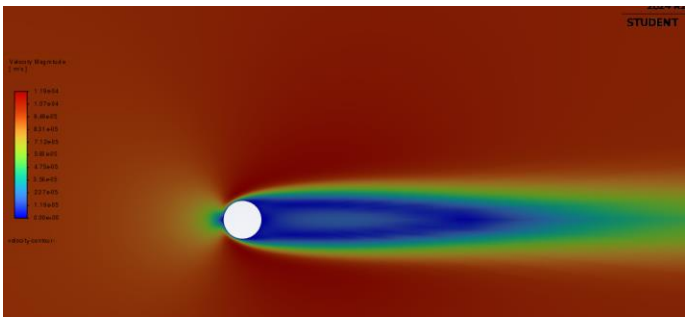

Figure 4 Velocity distribution

The velocity contours in literature are

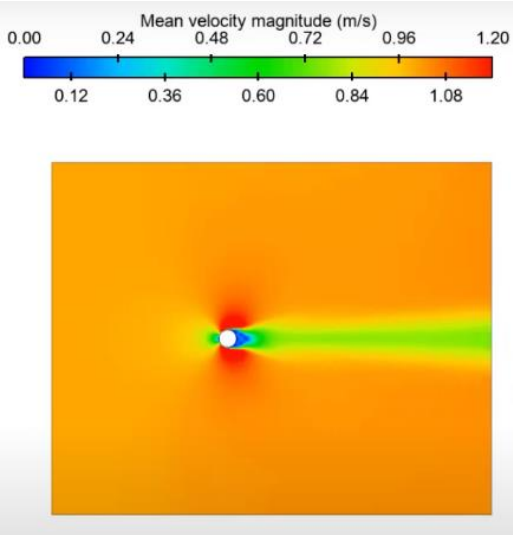

Figure 5 Exp velocity contours

Convergences

These graphs show how well the numerical solution satisfies the mass conservation equation, indicating the reduction of residuals over iterations or time steps. The residuals of the momentum equations (Navier-Stokes) in each direction, demonstrating the accuracy and stability of the velocity field solution. Convergence indicates the solution is approaching a steady or periodic state.

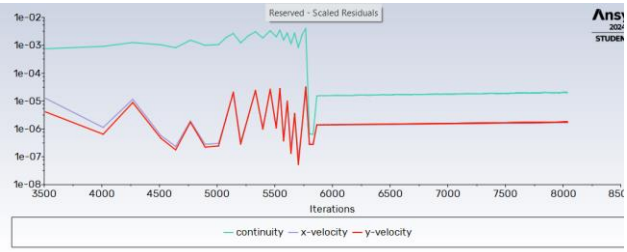

Figure 6 Convergence graph

Pressure Distribution

Pressure distribution contours illustrate how pressure varies around the cylinder, with high pressure at the stagnation point (front of the cylinder) and low pressure near the separation points (sides). This distribution directly influences lift and drag forces acting on the cylinder.

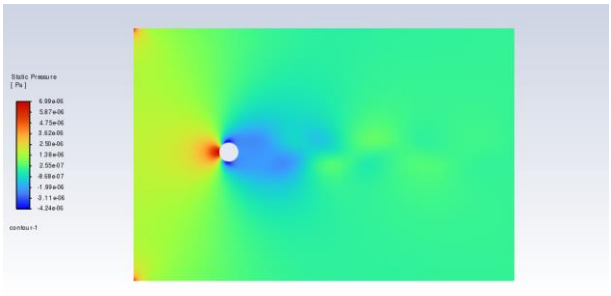

Figure 7 Static pressure

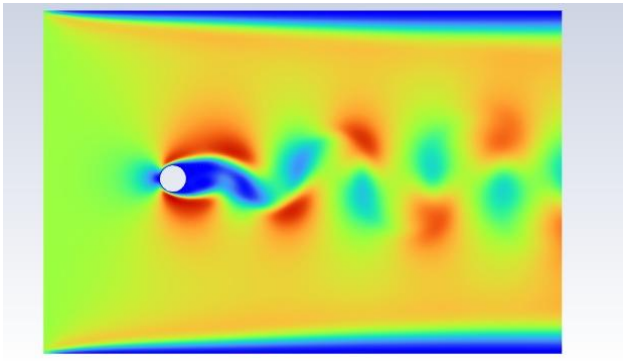

Figure 8 Dynamic pressure

The static and dynamic pressure distribution graphs are.

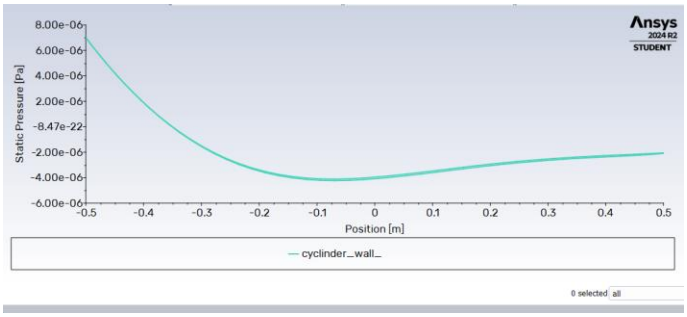

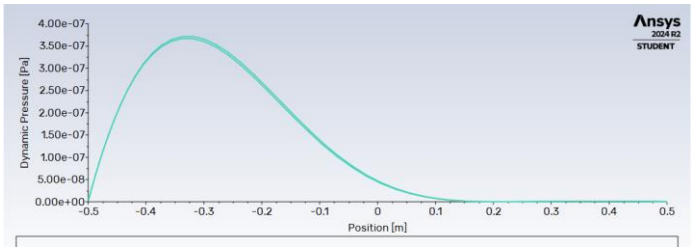

The pressure contours for experimental results are

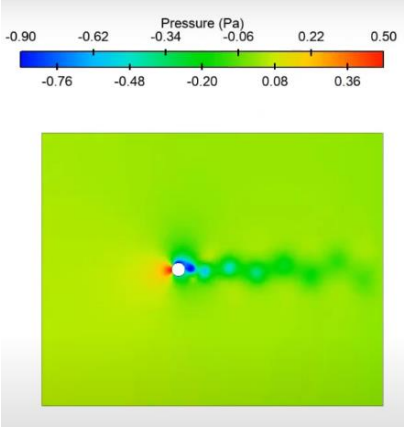

Figure 9 Exp Pressure contours

Pressure Coefficient C_p

The pressure coefficient quantifies the pressure variation on the cylinder's surface relative to the free-stream pressure. It helps assess flow behavior, including stagnation, separation, and aerodynamic forces like lift and drag.

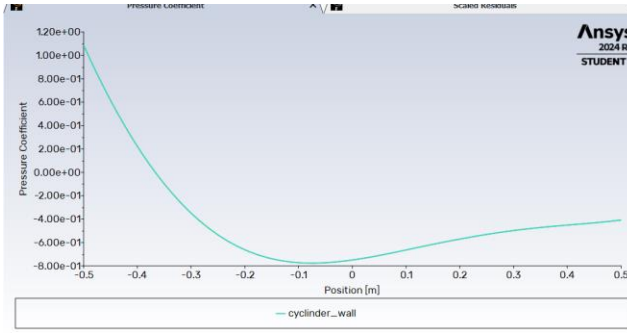

Figure 10 Pressure coefficient

The experimental pressure coefficient shows graph very similar to this one at $Re = 100$.

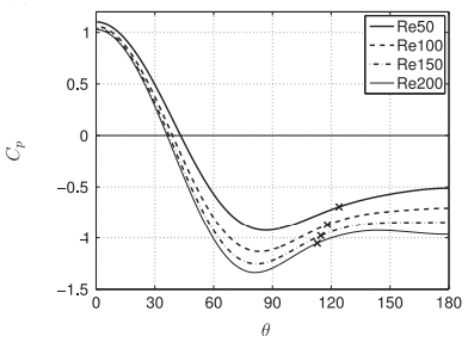

Figure 11 Experimental pressure coefficient[7]

Grid Independent Studies

The grid independent analysis was done to show that the results are independent of the grid sizing because the initial analysis was done at 50,000 element size and in this step the element size is set at **100,000 elements**, the mesh is generated, and the pressure field is again demonstrated to show the same results.

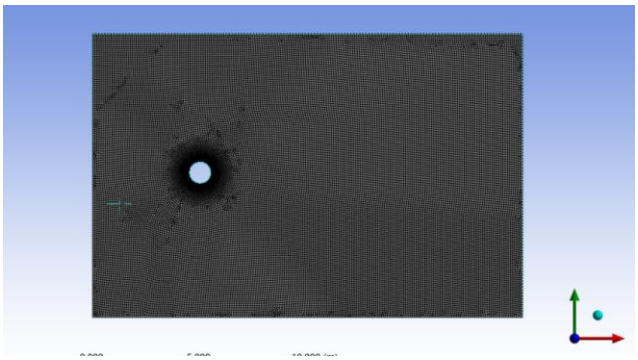

Figure 12 100,000 elements size

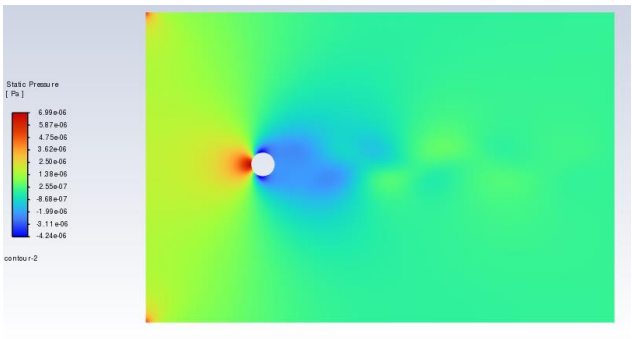

Figure 13 Pressure distribution at 100,000

Vorticity Contours

The rotational motion of fluid, highlighting regions of high shear and vortex formation. They reveal details about flow separation, wake dynamics [10], and vortex shedding patterns downstream of the cylinder.[11]

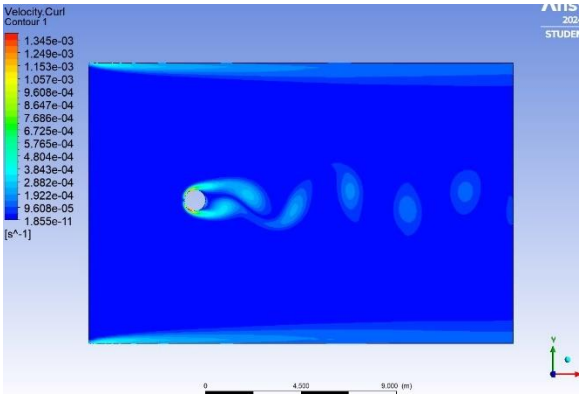

Figure 14 Vorticity Contours

Lift Coefficient C_L

shows how the lift force on the cylinder varies over time. For unsteady flow at $Re = 100$, it typically exhibits periodic oscillations due to alternating vortex shedding, which corresponds to the Strouhal number.

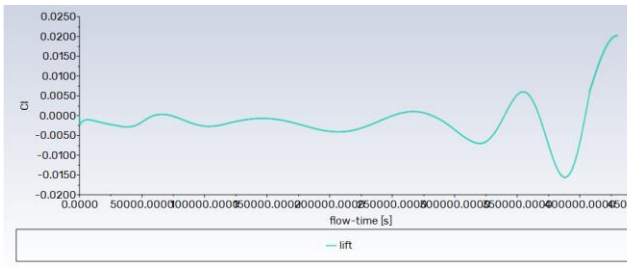

Figure 15 Lift coefficient

Drag Coefficient C_D

Illustrates the drag force on the cylinder as a function of time. At $Re = 100$, it shows negligible fluctuations superimposed on a steady mean value, with variations corresponding to the periodic vortex shedding in the wake.

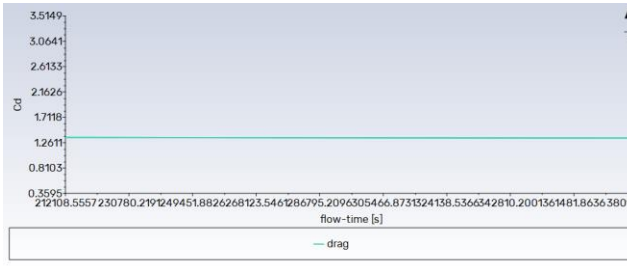

Figure 16 Drag coefficient

In experimental graphs we can observe the oscillation with respect to time.

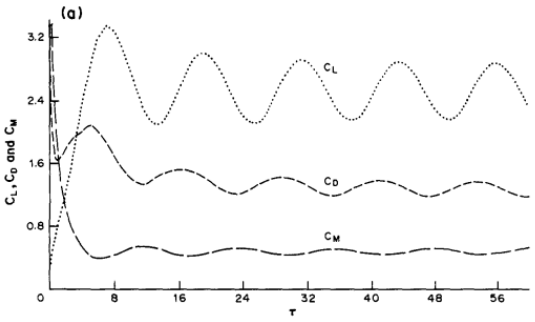

Figure 17 Experimental C_L[5]

Root mean sq C_L & $\overline{C_D}$

The root mean square coefficient of lift is $\mathbf{1.486 \times 10^{-6}}$ and average drag coefficient is $\mathbf{1.295}$

The average C_D value from literature at $Re = 100$ is 1.32

Table 1
Comparison of flow quantities with earlier numerical results; Re = 100.

Author(s) (year)	$-C_{pb}$	C_{Dp}	C_D
Park et al. (1998)	0.725	0.99	1.33
Kravchenko and Moin (1998)	0.73	0.99	1.32
Shi et al. (2004)	–	–	1.318
Mittal (2005)	–	–	1.322
Stålberg et al. (2006)	–	0.972	1.32
Posdziech and Grundmann (2007)	0.709	–	1.325
Li et al. (2009)	0.701	0.995	1.336
Present, D9	0.709	0.984	1.319

Figure 18 Experimental drag coefficient[7]

Strouhal Number

The graph reveals the dominant vortex shedding frequency. A sudden decrease in amplitude indicates a sharp drop in energy contribution at frequencies beyond the primary shedding frequency, signifying the periodicity and coherence of vortex shedding.

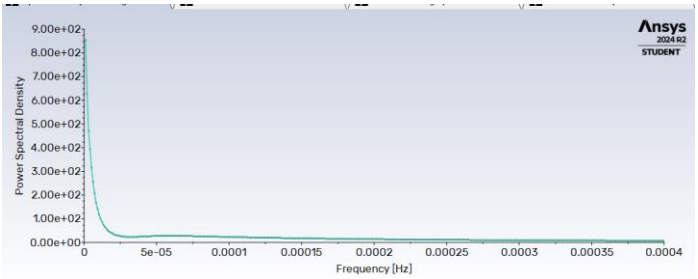

Figure 19 Strouhal Graph

The experimental Strouhal Graph shows exact variation.

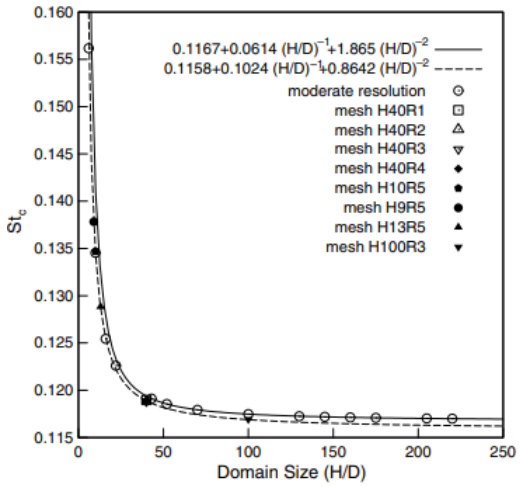

Figure 20 Experimental Strouhal No.[6]

Conclusions

1. **Validation of Results:** The simulation of 2D unsteady incompressible flow past a circular cylinder at $Re = 100$ successfully replicated key flow characteristics, including vortex shedding and pressure distribution, with results for C_p, C_L, C_D and Strouhal number in good agreement with literature values.
2. **Velocity Field and Boundary Layer Behavior:** The velocity contours accurately captured flow acceleration near the stagnation point, flow separation at the rear, and wake development downstream, showcasing the reliability of the computational setup.
3. **Pressure and Vorticity Distribution:** Pressure contours demonstrated high and low-pressure regions consistent with theoretical expectations, while vorticity contours highlighted flow separation and periodic vortex shedding in the wake region.
4. **Coefficient Analysis:** The calculated time-averaged drag coefficient $\overline{C_D}$ and root mean square of the lift coefficient C_L matched well with benchmark studies, validating the numerical methodology and grid-independent results.
5. **Flow Periodicity and Strouhal Number:** The periodic nature of vortex shedding, as seen in the oscillations of C_L and frequency spectra, confirmed the computed Strouhal number's consistency with established values, ensuring the robustness of the simulation and analysis.

Bibliography

[1] S. Mossaz, P. Jay, and A. Magnin, "Two-dimensional unsteady inertial flows of a yield stress fluid around a cylinder," *J Nonnewton Fluid Mech*, vol. 295, p. 104623, Sep. 2021, doi: 10.1016/J.JNNFM.2021.104623.

[2] T. Tang, H. Zhu, Q. Chen, G. Li, and T. Zhou, "CFD analysis of flow-induced rotation of a circular cylinder with a detached rear splitter plate in laminar flow," *Ocean Engineering*, vol. 266, p. 112703, Dec. 2022, doi: 10.1016/J.OCEANENG.2022.112703.

[3] S. Sun, W. Yang, S. Liu, P. Li, and M. C. Ong, "Computational fluid dynamics simulations of a near-wall rectangular cylinder in an oscillatory flow," *Ocean Engineering*, vol. 304, p. 117776, Jul. 2024, doi: 10.1016/J.OCEANENG.2024.117776.

[4] S. E. Rogers and D. Kwak, "An upwind differencing scheme for the incompressible navier–strokes equations," *Applied Numerical Mathematics*, vol. 8, no. 1, pp. 43–64, Aug. 1991, doi: 10.1016/0168-9274(91)90097-J.

[5] H. M. Badr, S. C. R. Dennis, and P. J. S. Young, "Steady and unsteady flow past a rotating circular cylinder at low Reynolds numbers," *Comput Fluids*, vol. 17, no. 4, pp. 579–609, Jan. 1989, doi: 10.1016/0045-7930(89)90030-3.

[6] B. Kumar and S. Mittal, "Prediction of the critical Reynolds number for flow past a circular cylinder," *Comput Methods Appl Mech Eng*, vol. 195, no. 44–47, pp. 6046–6058, Sep. 2006, doi: 10.1016/J.CMA.2005.10.009.

[7] L. Qu, C. Norberg, L. Davidson, S. H. Peng, and F. Wang, "Quantitative numerical analysis of flow past a circular cylinder at Reynolds number between 50 and 200," *J Fluids Struct*, vol. 39, pp. 347–370, May

2013, doi: 10.1016/J.JFLUIDSTRUCTS.2013.02.007.

[8] D. Luo, Y. Bai, and Z. Wang, "Numerical study on the flow control mechanisms of an off-surface circular cylinder for wall-bounded flows with separation," *Ocean Engineering*, vol. 294, p. 116729, Feb. 2024, doi: 10.1016/J.OCEANENG.2024.116729.

[9] S. K. Pandit and P. Das, "A novel transformation free nonuniform higher order compact finite difference scheme for solving incompressible flows on circular geometries," *European Journal of Mechanics - B/Fluids*, vol. 109, pp. 225–242, Jan. 2025, doi: 10.1016/J.EUROMECHFLU.2024.10.004.

[10] U. Ali, S. Khan, M. Islam, and I. Janajreh, "Modal Decomposition of Wake Flow Behind a Circular Cylinder," *Procedia Comput Sci*, vol. 241, pp. 338–344, Jan. 2024, doi: 10.1016/J.PROCS.2024.08.045.

[11] F. Zhao, Y. Zhou, F. Ren, H. Tang, and Z. Wang, "Mitigating the lift of a circular cylinder in wake flow using deep reinforcement learning guided self-rotation," *Ocean Engineering*, vol. 306, p. 118138, Aug. 2024, doi: 10.1016/J.OCEANENG.2024.118138.